Photodiagnosis and Photodynamic Therapy 27 (2019) 173–183

Contents lists available at ScienceDirect

Photodiagnosis and Photodynamic Therapy

journal homepage: www.elsevier.com/locate/pdpdt

PEGylated doped- and undoped-TiO_2 nanoparticles for photodynamic Therapy of cancers

Zahir Shah[a,b,c,*], Samina Nazir[d,**], Kehkashan Mazhar[e], Rashda Abbasi[e], Igor M. Samokhvalov[a,b,c]

[a] Guangzhou Institutes of Biomedicine and Health, Chinese Academy of Sciences, Guangzhou, 510530, China
[b] Key Laboratory of Regenerative Biology, Chinese Academy of Sciences, Guangdong Provincial Key Laboratory of Stem Cells and Regenerative Medicine, Guangzhou, 510530, China
[c] University of Chinese Academy of Sciences, Beijing, 100049, China
[d] College of Science, King Faisal University, Al-Ahsa, Saudi Arabia
[e] Institute of Biomedical & Genetic Engineering (IBGE), Sector G-9/1, Islamabad, Pakistan

ARTICLE INFO

Keywords:
Titanium dioxide
Nanoparticles
Photodynamic therapy
Cancer
PEGylation
Phototoxicity

ABSTRACT

Titanium dioxide has been widely known for its phototoxicity in the environmental context, but little is known for its use in the photodynamic therapy of cancers. Previous studides have shown the hazardous effects of undoped-titanium dioxide nanoparticles (undoped-TiO_2 NPs) in the ecosystem; however, it remains to explore the effect of polyethylene glycol (PEG) conjugation and doping of metal and non-metal on the photodynamic activity of TiO_2. Here we report the synthesis, characterizations, and applications of doped- and undoped-TiO_2 NPs stabilized by PEG in the photodynamic therapy of cancers. Our results demonstrate that *in vitro* PEG-NPs significantly reduced the survival of human cervical cancer cells (HeLa) upon solar and ultraviolet (UV) radiations. We found that doping of the metal (cobalt) and non-metal (nitrogen) onto TiO_2 nanocrystals enhanced the photoactivation of doped-TiO_2 NPs in the visible/near infrared (Vis/NIR) region, but these nanocrystals were revealed by cytotoxicity assays to be less potent in killing cancer cells compared to PEGylated undoped-TiO_2. The significant photodynamic effect was shown by PEGylated undoped-TiO_2 synthesized through the sol-gel method with 75% killing of HeLa cells at 5.5 μg/mL concentrations in exposure to UV or sunlight radiations. *In vitro* cytotoxicity was measured by Sulforhodamine B (SRB) and 3-(4, 5-Dimethylthiazol-2-Yl)-2,5-Diphenyltetrazolium Bromide (MTT) assays after irradiations with IR, UV, and sunlight for 15–30 minutes (min). All the synthesized NPs were characterized by XRD, AFM, SEM, EDX and DRS chemical analysis. Taken together, our data demonstrate that water-soluble PEGylated TiO_2 NPs maybe a good candidate for the photodynamic therapy of cervical cancer cells. Our data propose that the use of PEG surfactant can enhance the potency of already available photochemical therpeutic agents.

1. Introduction

The rapid progression in nanomaterial (NM) research has increased novel diagnostic methods and treatment of diseases [1] due to the reduction in material size, which makes it more exposed to the environment *via* enhanced surface volume to mass ratio [2]. NMs have been widely used for their unique properties in a number of applications including drugs [3,4], gene-delivery and imaging [4–6], cancer cell diagnosis [7,8], tissue engineering [9], in delivery systems (by using specialized tags as peptide, protein, antibody, and gene therapy), and as a carrier drugs in pharmacokinetics and pharmacodynamics [10–12]. Multiple studies have explored the anti-tumor potential of NMs in photochemical therapy [13,14]. This has drawn greater attention as a therapeutic modality so that numerous photosensitizers have been currently implied in the clinical treatment of multiple cancer types [15,16]. Titanium dioxide (TiO_2), a well-known semiconductor has been used commercially in the water purification [17–19] and in self-cleaning material applications [20,21]. Due to its high band gap energy (3.0 eV for rutile phase and 3.2 eV for anatase phase), TiO_2 can only be activated with ultraviolet (UV) light, and only a small portion (˜5%) of the solar energy (< 390 nm) can be utilized in practical applications [22]. The modifications of TiO_2 to render its sensitivity to visible light has become one of the most important goals to increase the utility of TiO_2 in medical applications. It has been reported that the doping of

* Corresponding author at: Guangzhou Institutes of Biomedicine and Health, Chinese Academy of Sciences, Guangzhou, 510530, China.
** Corresponding author.
E-mail addresses: zahir@gibh.ac.cn (Z. Shah), ssamina@kfu.edu.sa (S. Nazir).

https://doi.org/10.1016/j.pdpdt.2019.05.019
Received 20 February 2019; Received in revised form 14 April 2019; Accepted 17 May 2019
Available online 25 May 2019

nonmetals [23–25] and metals [26–28] into the TiO_2 lattice have shifted the band gap to lower energy, particularly the substitution doping of nitrogen was found to be effective in narrowing the band-gap through the mixing of N with O-2p states [24]. In addition, most photosensitizers implicated in clinical or in pre-clinical systems have hydrophobic properties, which cannot be used in an aqueous system with ease, thus limiting their delivery and photosensitizing efficiency [29,30]. PEG has been used by many researchers to resolve the solubility issue of the hydrophobic NPs while folate receptor-targeted (FR-tagged) NPs have been shown to enhance the specificity of drug delivery systems and to prolong retention time and bioavailability within tumors [31]. However, the PEGylated, doped- and undoped-TiO_2 NPs have not been tested in the previous reports against cancer cells. To extend our previous study on the hazardous effects of unmodified TiO_2 NPs in the ecosystem [32], here we synthesized and modified TiO_2 NPs (PEGylated undoped-TiO_2 NPs, PEGylated doped-NPs, folate loaded NPs, and gold core-shell NPs) for the safer use in photodynamic therapy of cancer cells.

2. Materials and methods

2.1. Reagents

Polyethylene glycol (Merk, MW. 4000), folic acid (Merk), hydrogen tetrachloroaurate (III) trihydrate (Aldrich), MTT (Sigma), trypsin-EDTA (Invitrogen), dicyclohexyl carbodiimide (DCC), and Folic acid, *N-Hydroxy Succinimide* were purchased from Sigma Aldrich. Ethanol, dimethyl sulfoxide and dichloromethane were purchased from Merck. Titanium tetra-isopropoxide, oleic acid, sodium citrate, trioctylamine, Ascorbic acid, triphenylphosphine, phthalimide, diisopropyl azodicarboxylate. Tetrahydrofuran (THF) was freshly distilled over CaH_2 followed by sodium/benzophenone before use. Methylene chloride was distilled over CaH_2. Thionyl chloride toluene, ethyl acetate, and n-hexane were used as such. The water employed in all preparations was purified by a Milli-Q system (Millipore). AKA 254 nm or UVC (Sanko Denki, Model G30T8), IR (Kodak-Sigma, 660 W, model S-2270) were used to excite photosensitizers. Cell cultur materials included, ethanol (75%), media (DMEM 50/50 and RPMI 1640) with 10% FCS and 1% GPPS, PBS (1X), T25 and T75 flasks, 15 mL and 50 mL centrifuge tubes, trypsin, fixative (50% TCA), sulforhodamine B solution (SRB) 0.4% in 1% acetic acid, wash solution (1% Acetic acid solution), Tris base solution 10 mm (Sulforhodamine B Assay solubilization solution), 0.4% Trypan Blue stain (fresh & filtered) in phosphate buffered saline. hemocytometer, cover-slips, tally counter, inverted microscope, incubator, laminar flow hood, centrifuge, micropipettes (p20, p100, and p1000).

2.2. Synthesis of titanium dioxide nanoparticles

Synthesis of the TiO_2 NPs was carried out according to the procedure given by Wang et al [33] with slight modifications. NPs were prepared by two synthetic routes either by an aqueous (Sol-gel) method or non-aqueous method. Briefly, in case of the sol-gel method, a solution prepared by ethanol and acetic acid (8:2) was added 50 mg TTIP under constant magnetic stirring at 50^0C for overnight, which transformed the mixture into a paste (semi-gel). The gel was dried at 120^0C and powdered. The product obtained was further used in the doping of 5% Co and 5% N. The doping of both Co and N was carried out by dropwise addition of Co and N precursor (solution in ethanol) into ethanol-acetic acid solution (8:2) containing TiO_2. The powder obtained was calcined at 500^0C for 6 h (Scheme 2).

A non-aqueous method was adapted to synthesized highly uniform TiO_2 nanocrystals (NCs), according to the procedure used by Gorden et al. [34] with several modifications. In brief, 7 mL oleic acid and 2 mL trioctylamine were mixed under constant stirring and heated to 120^0C for 1 h under N_2. The temperature was lowered to about 65-70^0C and 1.5 mL of 0.4 M (in ethanol) $TiCl_4$ was added and immediately heated to 300^0C for 10 min. The heating assembly was unplugged followed by a dropwise addition of 3.5 mL of $TiCl_4$ stock solution that continued for overnight aging. The solution was added toluene and centrifuged at 1000 rpm for 5 min to settle down the large particles. The supernatant was added methanol and centrifuged at 6000 rpm for 5 min, followed by chloroform and centrifuged for 5 min at 6000 rpm. The supernatant was evaporated by heating and dried particles were powdered and calcined at 500^0C for 6 h.

2.3. Gold titania core-shell NPs synthesis

In order to synthesize the gold core-shell TiO_2 NPs, firstly hydrogen tetrachloroaurate (III) trihydrate [$HAuCl_4.3H_2O$], 0.01 M ascorbic acid was mixed with 0.01 M sodium citrate under vigorous stirring for 5 min and a solution containing 50 mL ethanol and 10 mL TTIP (0.04 M) was added and incubated overnight under constant stirring. The solution was heated to 50^0C to transform into a gel. The gel was dried at 120^0C and calcined at 500^0C for 6 h.

2.4. Organic linker synthesis

2.4.1. Synthesis of PEO-di-phthalimide (Mitsunobu reaction)

Organic synthesis of the polyethylene glycol bis-amine (PEG-$(NH_2)_2$ was carried out according to the mechanism proposed by Mitsunobu [35]. In brief, $PEG_{n=}4000$ (20 g), triphenylphosphine (4 g), phthalimide (2.2 g), THF (100 mL) and 3 mL ethanol were mixed together with N_2 assembly at 30^0C under constant stirring and was added 3 mL (15 mmol) diisopropyl azodicarboxylate (DIAD) dropwise and continued to stir for 72 h. The reaction mixture was added 250 mL ethanol under the stirring condition for an additional1 h and the oily product was obtained through rotary evaporation at 40^0C. The product was confirmed by Fourier transform infrared spectrometer (FTIR) and nuclear magnetic resonance spectroscopy (NMR) (Scheme 1, Fig. 1C).

In the second step, PEG-di-phthalimide (17 g) and hydrazine monohydrate aqueous (17 mL, 80%) was added to ethanol (120 mL) and stir under N_2 atmosphere and refluxed for 12 h. Byproducts were precipitated by adding 3 mLconcentrated HCl, filtered and rotory evaoparted. Theoily amino-PEG obtained was washed, rotory evaportaedand finally dried at 40^0C under high vacuum, that yielded an off-white powder. The product was confirmed by FTIR and NMR (Scheme 1, Fig. 1D,E).

2.4.2. Synthesis of activated folate-conjugated PEG

Folic acid (0.250 g) dissolved in DMSO (12 mL), triethylamine (0.125 mL) and, N-hydroxysuccinimide (NHS) (0.13 g) and dicyclohexylcarbodiimide (DCC) (0.125 g), were mixed together and stirredin dark for 24 h under N_2 atmosphere. The mixture was and evaporated under reduced pressure to remove byproducts. The product was characterized by FT-IR (Fig. S1) and stored at -20^0C.

2.4.3. Synthesis of folate-polyethyleneglycol bisamine

Folate-conjugated PEG was synthesized by using an N-hydroxysuccinimide ester of folic acid (FA-NHS). PEG bis-amine (MW 4000) and FA-NHS were dissolved separately in dry DMF and mixed together and diisopropylethylamine was added. The mixture was allowed to react at room temperature for 24 h under an N_2 atmosphere. The solvent was rotory evaporated, that gave us a pale yellow product. The product was confirmed by ^{1}H NMR (Supplementary Fig. 1).

2.4.4. Conjugation of folate to (PEG-$NH_2)_2$) and to NPs

In the final step, polyethylene glycol was conjugated with the above targeting moiety to produce a good delivering system. TiO_2 doped and core-shell NPs were mixed with folate conjugated PEG in a conical flask wrapped in aluminum foil in dark with constant stirring for 24 h. The folate conjugated NPs were centrifuged at 1300 rpm for 5 min and the

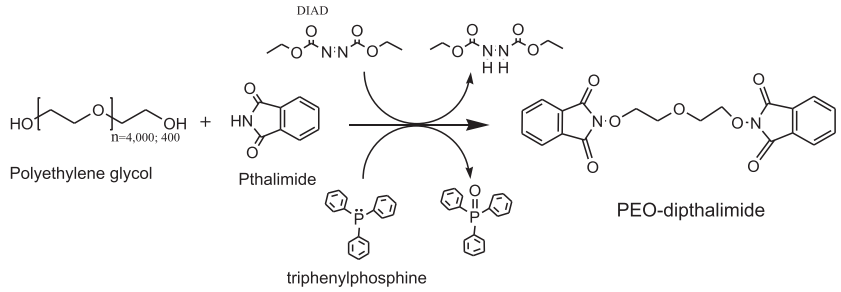

Synthesis of PEG-dipthalimide, anintermediate in the sythesis of NH_2-PEO-NH_2

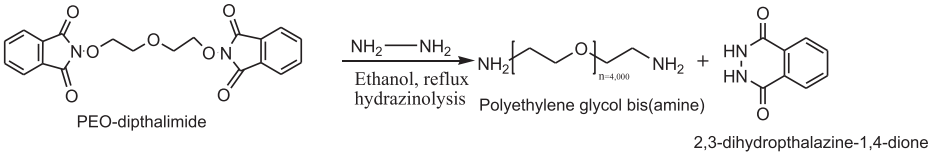

Hydrazinolysis of PEG-dipthalimide into PEG-bis(amine)

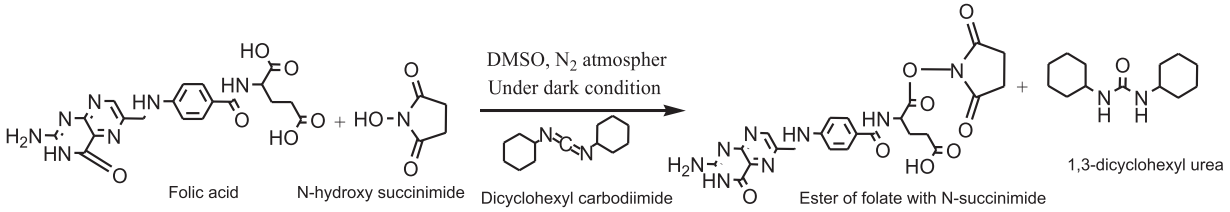

Folic acid activation for conjugation with PEG-bis(amine)

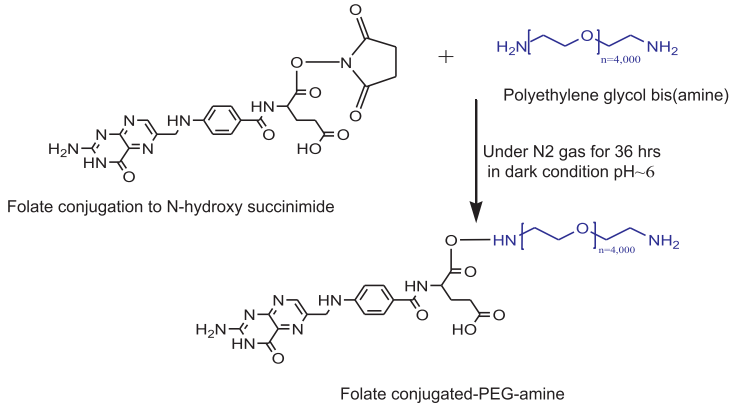

Scheme 1. Schematic route of PEG-bis(amine) linker synthesis to the final folate conjugated -PEG amine.

supernatant was discarded. Functionalized NPs were dried and stored at room temperature for *in vitro* analysis.

2.5. In vitro Analysis of cancer lines

2.5.1. Cell culture

All *in vitro* cell culture assays experiments were performed using human cervical cells (HeLa) and human skin cancer cells (HT144) according to the applied protocol at Institute of Biomedical & Genetic Engineering, Islamabad, Pakistan (IBGE). Both cell lines were tested for mycoplasma on regular basis to avoid any contamination. Cell lines were maintained in 45% Dulbecco's Modified Eagle Medium (DMEM) and 45% Roswell Park Memorial Institute (RPMI) and 10% FCS containing 1% gentamicin, penicillin, streptomycin (GPPS) antibiotics and split upon ≥90% confluence in T-flask.

2.5.2. Cytotoxicity measurement

In vitro cytotoxicity of the doped-and undoped-TiO NPs was measured by Sulforhodamine B (SRB) and 3-(4,5-Dimethylthiazol-2-Yl)-2,5-Diphenyltetrazolium Bromide (MTT) assays after irradiations with IR, UV, and sunlight for 15–30 minutes (min). Cytotoxicity of the doped-and undoped-TiO NPs have been investiagted

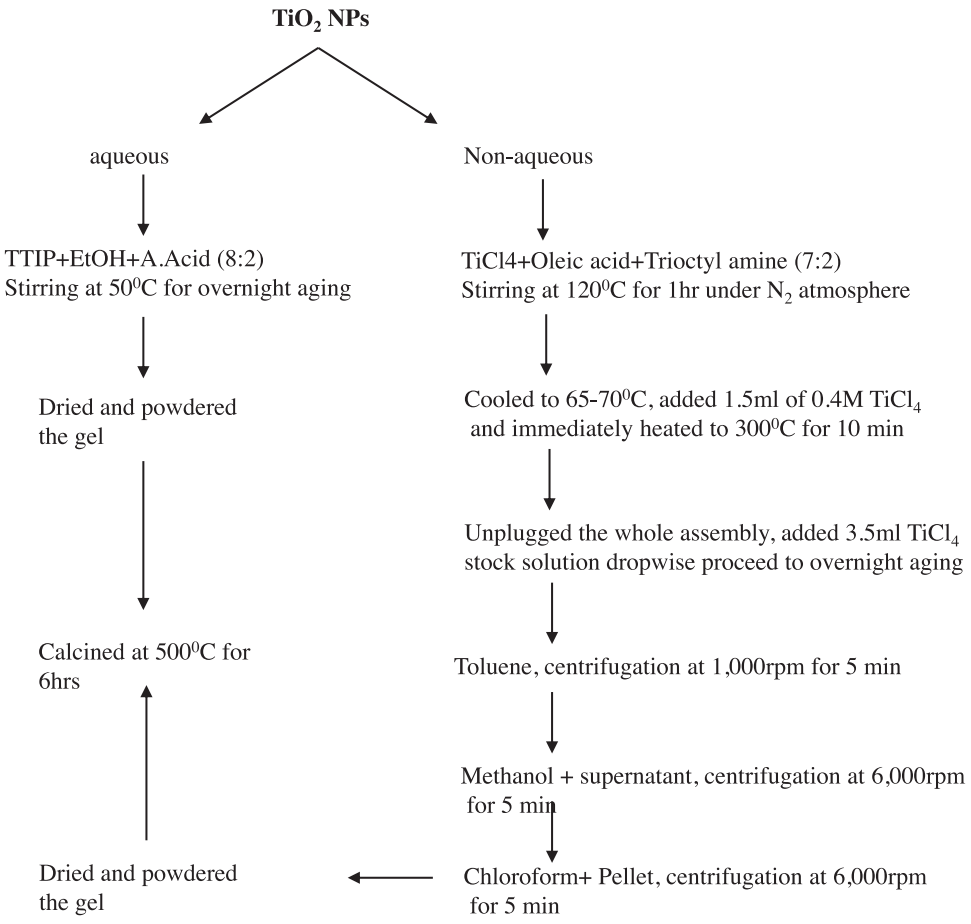

Scheme 2. Sketch of TiO_2 NPs synthesis through aqueous and non-aqueous routes.

3. Results

3.1. Characterizations of doped and undoped-TiO_2 NPs

Previous studies demonstrated the phototoxicity of TiO_2 NPs [36,32] in its unmodified form, however, it remained to explore the effect of metal and non-metals doping onto the TiO_2 NPs phototoxicity. The TiO_2 NPs were synthesized by aqueous and non-aqueous routes and calcined at 500^{0}C for 6 h in order to check the effect of the solvent on particle size and its absorption property. XRD analysis was used to identify the crystalline structure of NPs for 2θ diffraction angles ranges from 0˚ to 80˚. Peaks analysis revealed the diffraction planes of crystalline anatase TiO_2 at 25.3˚, 37.8˚, 48˚, 62.7˚, and 55˚ (Fig. 2A, [37]), while peaks at 53.8˚, 68.7˚, and 70˚ were attributed to diffraction planes of crystalline rutile TiO_2. We found no significant effect on the absorption of the TiO_2 NPs synthesized through both aqueous ($TiO_{2\ aq}$) and non-aqueous ($TiO_{2\ non\text{-}aq}$) routes as shown by the XRD pattern (Fig. 2A(a,g,h)). Overall diffractograms of the undoped-TiO_2 NPs showed the presence of mainly anatase TiO_2 nanocrystalsand are in close agreement with the standard spectra's [37–39]. Interestingly, all the doped-TiO_2 showed a shift from anatase into rutile crystalline structure, which can be seen from the shift of the highest peak (80) from short wavelength (25.3˚) for anatase to a longer wavelength for rutile in all the three doped-TiO_2 NPs (Fig. 2A(d–f)). XRD analysis revealed that both anatase and rutile mesoporous crystals are present in all the doped-NPs synthesized (Fig. 2A). Diffuse reflectance spectroscopy (DRS). Analysis revealed the shifting of absorption wavelength from UV to IR region, which verified the results obtained from XRD (Fig. 2A). The N, Co codoped- NPs showed the highest absorption compare to the single **N**-doped or Co-doped TiO_2 NPs. The topology of the NPs was investigated with high-resolution atomic force microscopy (AFM) Atomic force microscopy (AFM) showing a range of particle size from 20 to 50 nm (Fig. 2C, Supplementary Fig. A,B). The average size of NPs was calculated as 33 nm on the basis of line profile determination.

The morphology of the TiO_2 NPs and its derivatives were assessed by scanning electron microscopy (SEM). The SEM images of these NPs calcined at 500^{0}C showed overall an irregular particle size in the range of 18–60 nm (Fig. 2B, Supplementary Fig. S2). The average particle size calculated was 45 nm for N, Co-codoped-TiO_2, 68 nm for gold core-shell TiO_2-PEGylated (polymeric core shell of TiO_2), 56 nm for PEGylate folate loaded-TiO_2 (targeted polymeric NPs) and 48 nm for Co-doped-TiO_2. The increase in size of these NPs support the conjugation of PEG and the loading of PEGylated folate onto TiO_2 NPs. Enormous studies have shown the significant role of PEG-conjugated NPs in the solubility and bioavailability *in vivo* and *in vitro* [40,41]. The qualitative and quantitative elemental analysis of the given sample was determined by energy dispersive x-ray spectroscopy (EDX) for the N, Co-codoped-TiO_2 that contained all the doped elements. Analysis revealed the detection of three prominent elements at around 0.525, 4.508 and 6.924 keV, which were attributed to O_2, Ti and Co respectively (Fig. 3D). According to this technique, the cobalt was doped to ˜3% into the TiO_2 shell by mass. Furthermore, the Co-doped NPs consists of 52% O_2 and 45% TiO_2 (Table 1). Taken together, the characterizations showed the successful synthesis of un-doped and doped-TiO_2 and gold core-shell TiO_2 NPs.

3.2. Characterizations of linker polyethyleneglycol bis-(amine)

Conjugation of the PEG to the folic acid was achieved with the help of short chain polyethylene glycol bis-amine (PEG-$(NH_2)_2$) linker. Each

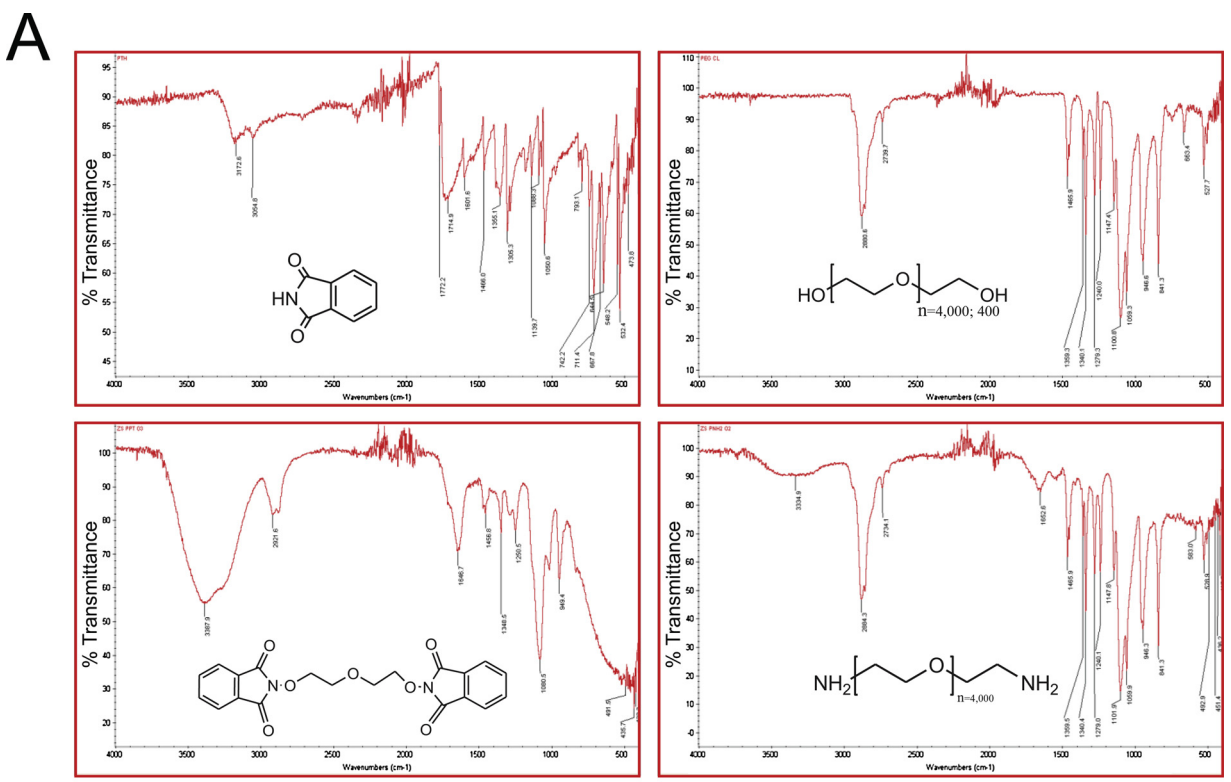

Fig. 1. Characterization of organic linker by FTIR and NMR.
(A–D) FTIR characterization of the initial substrates through the intermediate PEG-diphthalimide to the final linker polyethylene glycol bis-amine. (E) ^{1}H NMR characterization of the final product polyethylene glycol bis-amine.

step of the organic synthesis of the linker was followed by FTIR to analyze the product at every stage of synthesis. The FTIR spectra clearly showed the difference between the substrates, intermediates and the final product (Supplementary Fig. 1A–C). The final product was confirmed by the appearance of FTIR peak at ˜3400 characteristics of primary amino groups ($-CH_2$-NH_2), which was not seen in any startup substrates (Fig. 1D, E). The ^{1}HNMR results depicted the characteristic peaks for the polymer branch at 3.5 ppm, a primary amino group ($-CH_2$-NH_2) at 4.7 ppm with byproduct peaks at ≥7.5. All the chemical characterizations showed the synthetic confirmation of PEG-phthalimide, PEG-dichloride and finally our required product PEG-$(NH_2)_2$ (Fig. 1, supplementary Fig. 1). In summary, the FTIR and ^{1}HNMR results confirmed the successful synthesis of the intermediates and the final product.

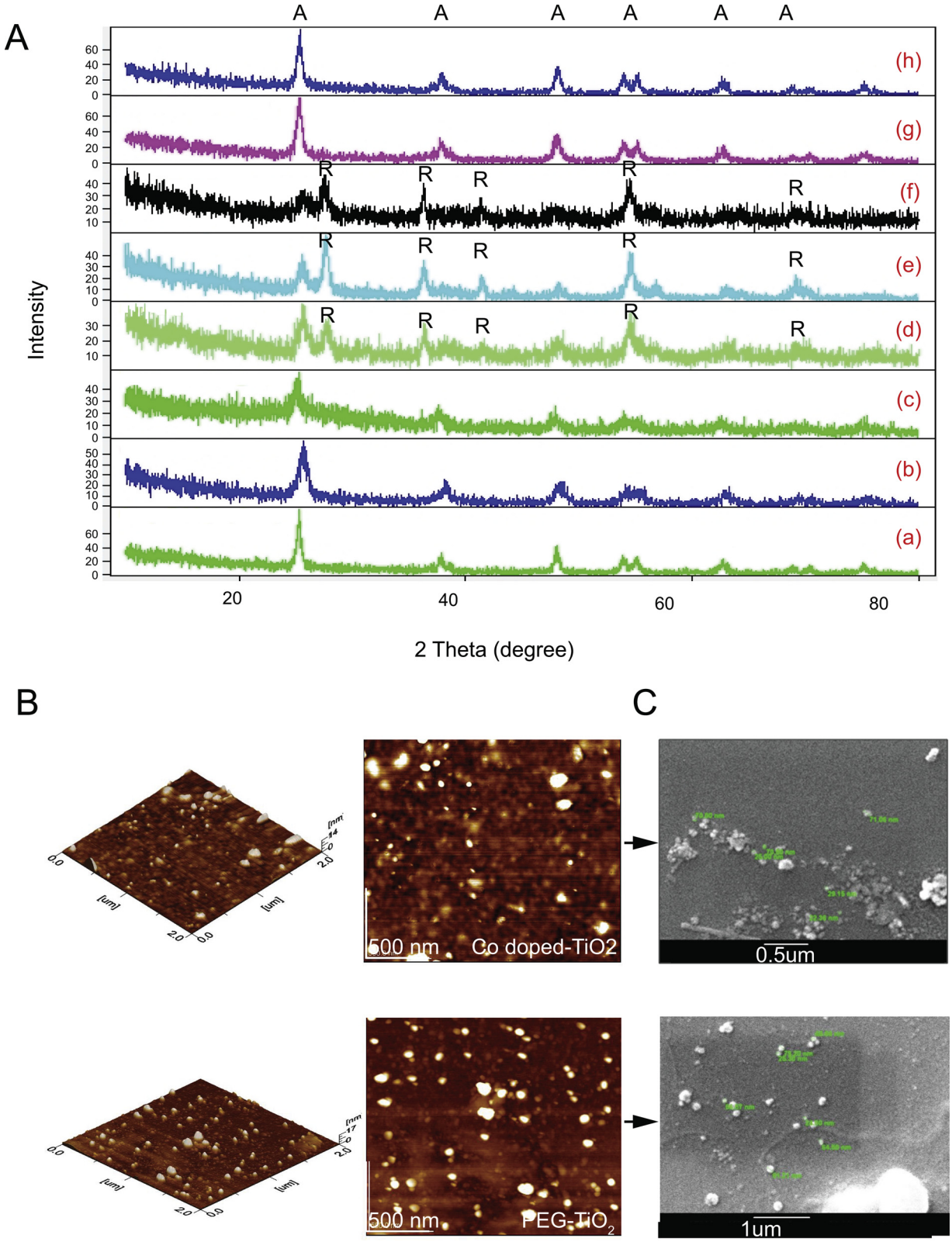

Fig. 2. Characterization of unmodified TiO_2 and modified NPs by XRD, AFM, and SEM.
(A) The XRD pattern shows the crystalline TiO_2 NPs and its derivative including $TiO_{2\ aq}$(a,h), Au core-shell PEG-TiO_2 (b), Au core-shell TiO_2 c) (N,Co)-codoped TiO_2 (d), N-doped TiO_2 (e), Co-doped TiO_2 (f) and $TiO_{2\ non\text{-}aq}$(g). (B–C) AFM and SEM images of PEGylated and doped TiO_2 NPs respectively.

3.3. Photodynamic therapy of cancer cells by doped and undoped-TiO_2 NPs

The toxicity of TiO_2 NPs has been documented by many studies. Recently, Garg et al. have shown the photocatalytic degradation of Bisphenol-A (BPA) by (N, Co)-codoped TiO_2 under visible light irradiations [39], however, the effect of such nanocomposite was not shown on cancer lines. In our study, we tried to use 1) PEG for the bioavailability 2) folate for the specific targeting and 3) metal and non-

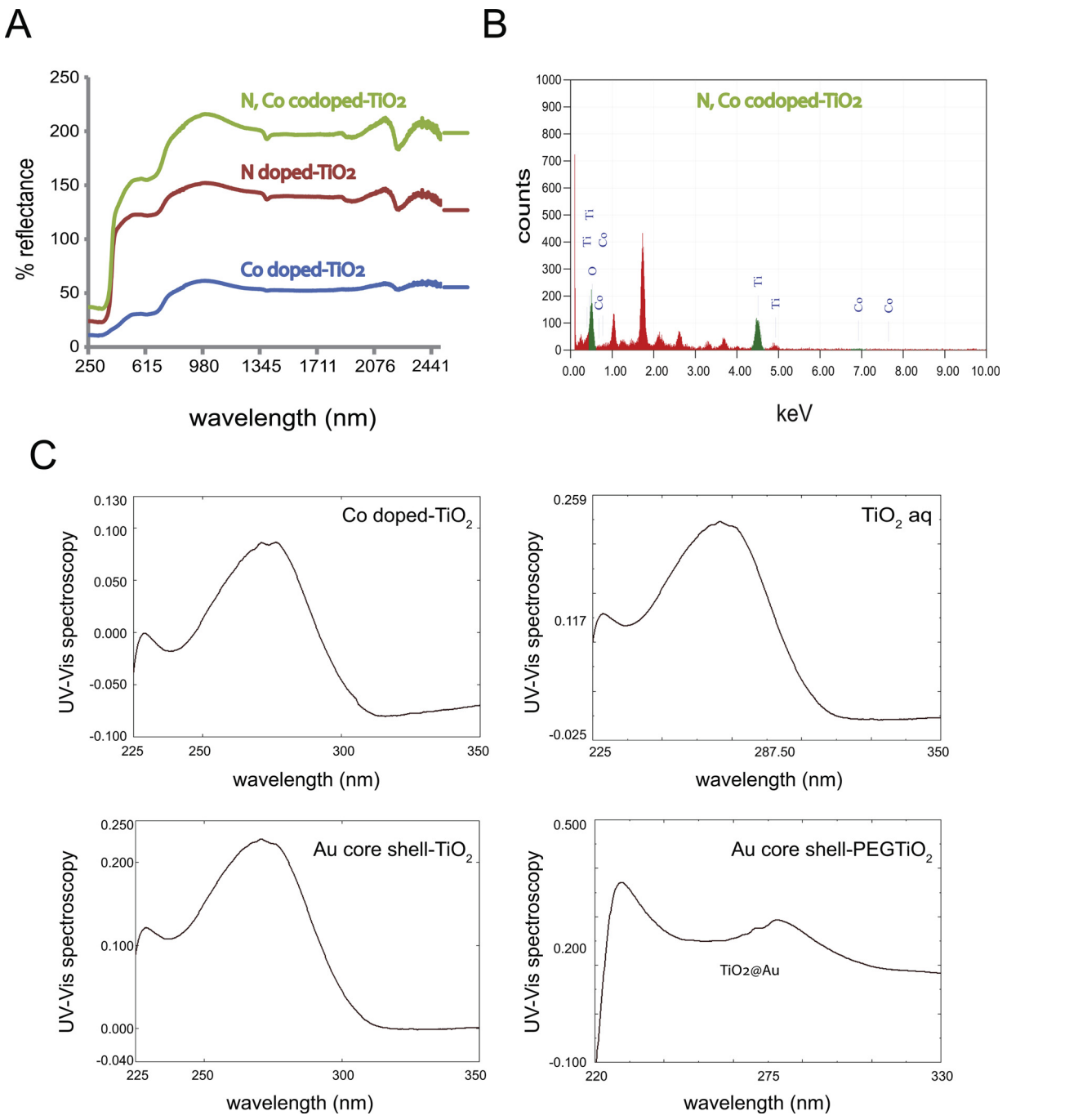

Fig. 3. Characterization of unmodified TiO_2 and modified NPs by DRS, EDX and UV–vis spectroscopy.
(A) Characteristics reflectance of metal and non-metal doped-TiO_2 NPs including Co-doped-TiO_2, N-doped TiO_2 and (N, Co)-codoped TiO_2. (B) Elemental analysis of the (N, Co)-codoped TiO_2. (C–F) UV–vis spectroscopy characteristics of $TiO_{2\ aq}$, Co-doped TiO_2, Au core-shell TiO_2, and Au core-shell PEG-TiO_2.

Table 1
Elemental analysis of NPs by EDX.

Elements	keV	Mass%	Atom%
O	0.525	52.22	76.78
Ti	4.508	45.10	22.15
Co	6.925	2.68	1.07

metal doping to shift the activation energy of TiO_2 NPs from UV into NIR and sunlight absorption range. The NPs were aimed to generate reactive oxygen species (ROS) inside the cells while damaging the nucleic acids that lead to programmed cell death (apoptosis) and necrosis after being endocytosed into the cells *via* glycosyl phosphatidylinositol-anchored glycoprotein [42–44]. The photodynamic effect of the newly synthesized NPs was tested on different cancer cell lines regularly cultures at IBGE. Generally, cells cultured to 85–90% confluence were added doped- and undoped-TiO_2, PEGylated-TiO_2 NPs at various concentrations (Fig. 4A, B) and photoactivated with a specific wavelength of radiations including IR, UV, and sunlight, leaving unexposed control in dark (wrapped in Aluminum foil) for the given time.

A total of 11 NPs (designated as #1 to #11, Supplementary Fig. 3) were subjected to preliminary cytotoxicity assay on the HT144 cancer cells to determine their potential in the photodynamic prevention of cancer cells. Cancer cells in the log phase were added the NPs and

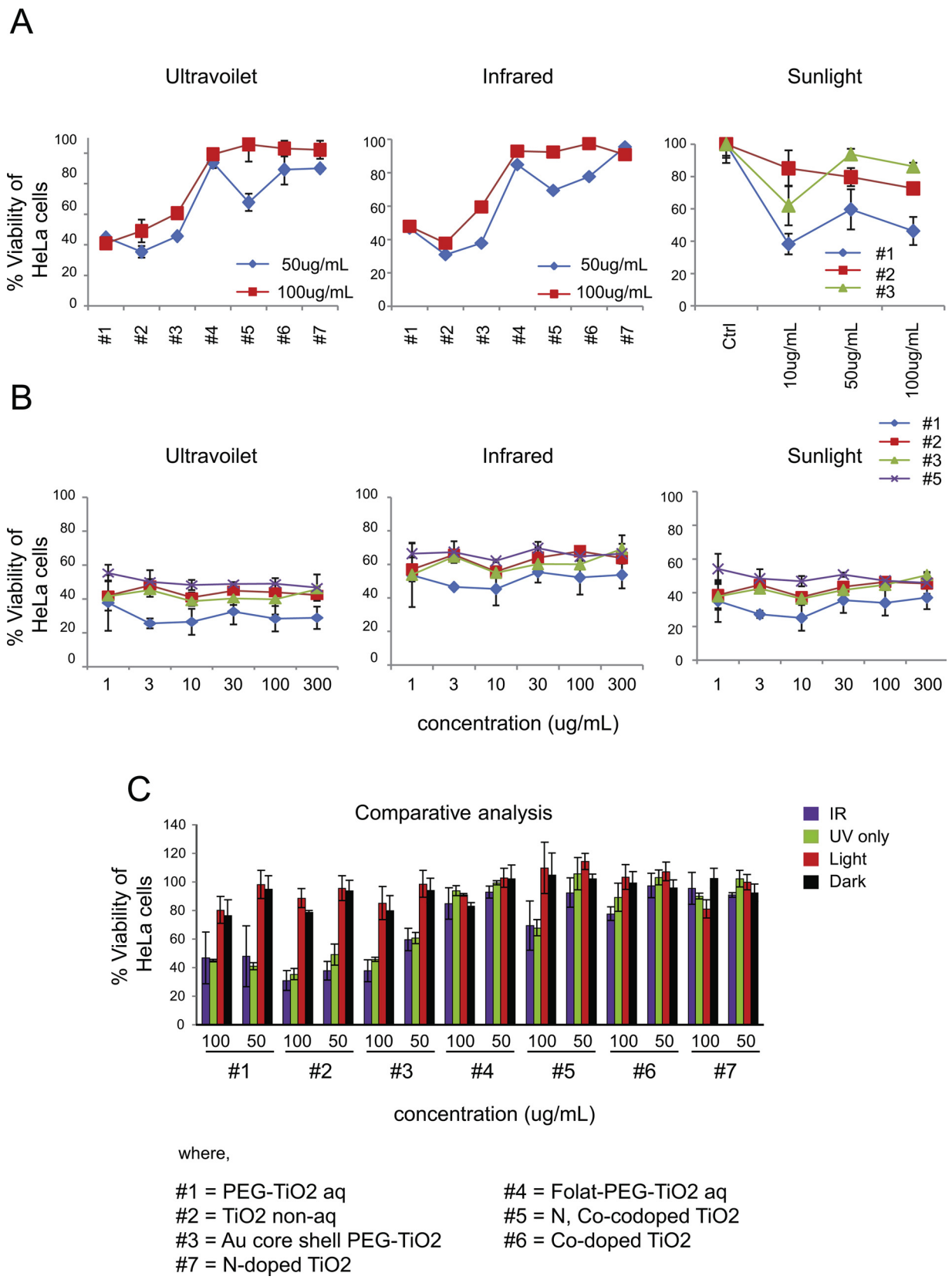

Fig. 4. *In Vitro* SRB and MTT cytotoxicity assays of modified and unmodified NPs.
(A) Phototoxicity of the seven newly synthesized NPs including #1-#7 against HeLa cancer cell upon exposure to ultraviolet (UV), infrared(IR) and sunlight (Light) radiations. (B) IC_{50} value determination for the potentialNPs against the cancer lines (C) Comparative analysis of all the all photoactivation radiation sources for all the seven NPs tested against HeLa cancer cells.

exposed to a specific wavelength of radiation for 15 min. Preliminary analysis by SRB cytotoxicity assay revealed the potential of several NPs in the photodynamic prevention of cancer cells (Supplementary Figure S3). In the first attempt, a total of seven NPs were selected including PEG-$TiO_{2\ aq}$, $TiO_{2\ non\text{-}aq}$, Au core-shell PEG-TiO_2, N-doped TiO_2, folate-PEG-$TiO_{2\ aq}$, N, Co-codoped TiO_2, Co-doped TiO_2 to be further tested on other cancer cells for their photodynamic effect. Cytotoxicity assay revealed that four NPs have repeated their cytotoxic effect on HeLa cancer cells in response to all the radiation sources (UV, IR, sunlight) used (Fig. 4, supplementary Fig. S3B), which is described below;

3.3.1. IR radiations

It has been shown that the TiO_2 can only be excited with exposure to UV radiations [45]. NPs were added to the cancer cells in log phase, and irradiated with IR source for 15 min and incubated at 37^0C for 24 h. The SRB analysis a reduction in cell viability of HeLa cells up to 30% for PEG-$TiO_{2\ aq}$ (100 μg/mL), 37% for $TiO_{2\ non\text{-}aq}$ (50 μg/mL) and gold core-shell PEG-TiO_2 (100 μg/mL) followed by N, Co-codoped TiO_2 (50, 100 μg/mL) (Fig. 4A). IC_{50} analysis also showed that PEG-$TiO_{2\ aq}$ has 45% reduced the HeLa cancer cells with IC_{50} valve 6.5 ± 4.95 μg/mL, followed by $TiO_{2\ non\text{-}aq}$ with 55.5% viability for 5.5 μg/mL ± 6.36, gold core-shell PEG-TiO_2 with 53.5% for 6.365.5 ± 6. 36 μg/mL and N, Co-codoped TiO_2 with 63% was 4.956.5 ± 4.95 μg/mL with 63% viability as shown in (Fig. 4B, Table 2),suggesting the safer use of this NPs in tumor patients.

3.3.2. UV radiations

The photosensitizers added cancer cells (HeLa) in log phase were UV irradiated for 15 min and the photo-toxicity was calculated. Again the PEG-$TiO_{2\ aq}$ NPs revealed a significant reduction of 25% in cancer cells viability (75% killing) for 5.5 ± 6.36 μg/mL calculated from IC_{50} analysis (Fig. 4B), followed by $TiO_{2\ non\text{-}aq}$ and gold core-shell PEG-TiO_2 with 39 viability (61% killing) for 6.365.5 ± 6.36 μg/mL and 20 ± 14 μg/mL respectively. N, Co-codoped TiO_2 again was the least potent in killing the cancer cells with 49% viability for 6.65 ± 4.95 μg/mL (Fig. 4, Table 2).

3.3.3. Sunlight radiations

Interesting results were found in case of sunlight exposure for 30 min (temperature ≤35^0C). In accordance to the UV effect, IC_{50} values for PEG-$TiO_{2\ aq}$ significantly killed the 75% cancer cells with 26% viability for IC_{50} value 4.6.5 ± 4.95 μg/mL, followed by $TiO_{2\ non\text{-}aq}$ with 35% viability at 5.5 ± 6.36 μg/mL, for gold core-shell PEG-TiO_2 was 5.5 ± 6.36 μg/mL with 36.5% viability and for N, Co-codoped TiO_2 was 4.96.5 ± 4.95 μg/mL with 47% viability (Fig. 4B). The p-value of sunlight exposed NPs showed a highly significant result *i.e.* $p \leq .001$ (Table 2). Taken together, our data demonstrate that the PEGylate $TiO_{2\ aq}$ synthesized by the sol-gel method resulted in an enhance photodynamic prevention of cancer cells, which dramatically reduced their viability under sunlight and infra-red radiations. This data may add a therapeutic agent in cancer photodynamic therapy for future therapy.

3.4. IC_{50} calculation inhibitory concentration at 50% inhibition

IC_{50} which is the inhibitory concentration at 50% inhibition was calculated using the manual method by Maes et al. (http://leishrisk.net/Leishrisk/UserFiles/File/Kaladrug-R/SOPs/lab/labSOP18_IC50tool.pdf). IC_{50} valves of four NPs (PEG-$TiO_{2\ aq}$, $TiO_{2\ non\text{-}aq}$, gold core-shell PEG-TiO_2 and N, Co-codoped TiO_2) were calculated on HeLa cell lines by MTT assay (Fig. 4B, Table 2), after irradiation with IR, UV and sunlight sources for 15 min.

3.5. Statistical analysis

Statistical significance was determined by ANOVA and two-tailed *t*-test between unexposed and irradiated samples (NPs). Results were considered significant when $p \leq 0.05$ and shown as mean ± SD.

4. Discussion

Cancers are the most life-threatening health problems (23.2%) in the world after heart disease (25.4%) and are the leading cause of mortality worldwide, both in developed and developing countries [46,47]. The current therapies for cancer suffer from many limitations as reviewed [48]. Nanoparticles (NPs) have shown several improvements for the development of functionalized anticancer agents in delivery systems by using specialized tags (peptide, protein, antibody, and gene therapy) as well modified the pharmacokinetics, pharmacodynamics of carrier drug [10,11]. To extend our previous studies on the phototoxic effects unmodified TiO_2 NPs [32], in this study, we demonstrated the effects of PEGylated-TiO_2 NPs, N, Co-codoped, Co-doped, N-doped TiO_2 NPs and gold core-shell NPs. These NPs were further used to be functionalized with loading PEGylated-folate. Surface modifications of NPs with surfactants (PEG) to achieve long-circulating nanocarriers have now been accepted as a standard strategy for targeted drug delivery (*in vitro* and *in vivo*) [49]. Initial analysis revealed that four NPs including PEG-$TiO_{2\ aq}$, $TiO_{2\ non\text{-}aq}$, gold core-shell PEG-TiO_2 (Au core-shell PEG-TiO_2) and N, Co-codoped TiO_2 showed their phototoxic effect on cancer lines, which were used in this study. Cytotoxicity of these NPs was measured by the standard cytotoxic SRB and MTT assays, which have been routinely used for the percent viability of cultured cells in our laboratory.

Comparative analysis revealed the significant effect of the PEGylated NPs (PEG-$TiO_{2\ aq}$), which was conjugated with short-chain PEG that probably enhanced its bioavailability and cell permeability as described by others (Fig. 4C [49]). Interestingly, these NPs not only showed prevention of cancer cells in response to UV radiations but the same effect was observed when exposed to sunlight for just 30 min. We observed that although the doping of Co (metal) and N (non-metal) or the co-doping of both the Co and N, enhanced the photoexcitation of the NPs in the IR and NIR regions, however, they did not show better phototoxic effect on cancer lines (Fig. 4A–C), which may be attributed to the downregulated of ROS production by these NPs or hindrance to cross the cell and nuclear membrane permeability. Loading of NPs with folic acid also did not enhance the photodynamic prevention of cancers by TiO_2 NPs, could be possibly due to an increase in additive size and charge on the NPs.

In sum, these data demonstrate the enhancement of the solubility effect of PEGylate TiO_2 that upon photoactivation can kill the cancer cells compared to un-PEGylated TiO_2 NPs. In the present study, the main objective was to use the phototoxicity of the TiO_2 NPs for cancer

Table 2
IC_{50} and % viability of cancer cells.

Light source	ZS1			ZS2			ZS3			ZS5		
	IC_{50}	S.D.	%viability	IC_{50}	S.D.	%viability	IC_{50}	S.D.	%viability	IC_{50}	S.D.	%viability
UV	5.5	6.36	25.5	5.5	6.36	39.5	20.0	14.2	39	6.6	4.95	49
IR	6.5	4.94	45.5	5.5	6.43	55.5	5.5	6.36	53.5	6.5	4.95	63
Sunlight	6.5	4.95	26.0	5.5	6.46	35	5.5	6.44	36.5	6.5	4.95	47

PDT and give an insight to the researchers for the safer use of TiO_2 NPs for the prevention of cancers.

Acknowledgment

Authors thank to the Deanship of Research, King Faisal University, Saudi Arabia, for the financial support and technical help in manuscript preparation. We would also like to thank Dr. Sher Wali, Chemistry department, Quaid-e-Azam University, Islamabad, Pakistan and Mr. Yogesh Srivastava, Guangzhou Institutes of Biomedicine and Health, Chinese Academy of Sciences, China for technical assistance in manuscript prepration.

This research did not receive any specific grant from funding agencies in the public, commercial, or not-for-profit sectors.

Appendix A. Supplementary data

Supplementary material related to this article can be found, in the online version, at doi:https://doi.org/10.1016/j.pdpdt.2019.05.019.

References

[1] Y. Liu, H. Miyoshi, M. Nakamura, Nanomedicine for drug delivery and imaging: a promising avenue for cancer therapy and diagnosis using targeted functional nanoparticles, Int. J. Cancer 120 (12) (2007) 2527–2537, https://doi.org/10.1002/ijc.22709.

[2] B.D. Chithrani, A.A. Ghazani, W.C. Chan, Determining the size and shape dependence of gold nanoparticle uptake into mammalian cells, Nano Lett. 6 (4) (2006) 662–668, https://doi.org/10.1021/nl052396o.

[3] M.M. Shenoi, N.B. Shah, R.J. Griffin, G.M. Vercellotti, J.C. Bischof, Nanoparticle preconditioning for enhanced thermal therapies in cancer, Nanomedicine Lond. (Engl.) 6 (3) (2011) 545–563, https://doi.org/10.2217/nnm.10.153.

[4] R.K. Visaria, R.J. Griffin, B.W. Williams, E.S. Ebbini, G.F. Paciotti, C.W. Song, J.C. Bischof, Enhancement of tumor thermal therapy using gold nanoparticle-assisted tumor necrosis factor-alpha delivery, Mol. Cancer Ther. 5 (4) (2006) 1014–1020, https://doi.org/10.1158/1535-7163.mct-05-0381.

[5] L. Li, Y. Wen, Q. Xu, L. Xu, D. Liu, G. Liu, Q. Huang, Application of carbon nanomaterials in gene delivery for endogenous RNA interference in vitro and in vivo, Curr. Pharm. Des. 21 (22) (2015) 3191–3198.

[6] A. Karmakar, S.M. Bratton, E. Dervishi, A. Ghosh, M. Mahmood, Y. Xu, L.M. Saeed, T. Mustafa, D. Casciano, A. Radominska-Pandya, A.S. Biris, Ethylenediamine functionalized-single-walled nanotube (f-SWNT)-assisted in vitro delivery of the oncogene suppressor p53 gene to breast cancer MCF-7 cells, Int. J. Nanomedicine 6 (2011) 1045–1055, https://doi.org/10.2147/ijn.s17684.

[7] X. Wu, H. Liu, J. Liu, K.N. Haley, J.A. Treadway, J.P. Larson, N. Ge, F. Peale, M.P. Bruchez, Immunofluorescent labeling of cancer marker Her2 and other cellular targets with semiconductor quantum dots, Nat. Biotechnol. 21 (1) (2003) 41–46, https://doi.org/10.1038/nbt764.

[8] A. Mukerjee, A.P. Ranjan, J.K. Vishwanatha, Combinatorial nanoparticles for cancer diagnosis and therapy, Curr. Med. Chem. 19 (22) (2012) 3714–3721.

[9] L.R. Hirsch, R.J. Stafford, J.A. Bankson, S.R. Sershen, B. Rivera, R.E. Price, J.D. Hazle, N.J. Halas, J.L. West, Nanoshell-mediated near-infrared thermal therapy of tumors under magnetic resonance guidance, Proc Natl Acad Sci U S A 100 (23) (2003) 13549–13554, https://doi.org/10.1073/pnas.2232479100.

[10] S. Parveen, R. Misra, S.K. Sahoo, Nanoparticles: a boon to drug delivery, therapeutics, diagnostics and imaging, Nanomedicine 8 (2) (2012) 147–166, https://doi.org/10.1016/j.nano.2011.05.016.

[11] R. Ranganathan, S. Madanmohan, A. Kesavan, G. Baskar, Y.R. Krishnamoorthy, R. Santosham, D. Ponraju, S.K. Rayala, G. Venkatraman, Nanomedicine: towards development of patient-friendly drug-delivery systems for oncological applications, Int. J. Nanomedicine 7 (2012) 1043–1060, https://doi.org/10.2147/ijn.s25182.

[12] J. Khandare, M. Calderon, N.M. Dagia, R. Haag, Multifunctional dendritic polymers in nanomedicine: opportunities and challenges, Chem. Soc. Rev. 41 (7) (2012) 2824–2848, https://doi.org/10.1039/c1cs15242d.

[13] W.G. Roberts, M.K. Klein, M. Loomis, S. Weldy, M.W. Berns, Photodynamic therapy of spontaneous cancers in felines, canines, and snakes with chloro-aluminum sulfonated phthalocyanine, J. Natl. Cancer Inst. 83 (1) (1991) 18–23.

[14] S. Ma, J. Zhou, Y. Zhang, B. Yang, Y. He, C. Tian, X. Xu, Z. Gu, An oxygen self-sufficient fluorinated nanoplatform for relieved tumor hypoxia and enhanced photodynamic therapy of cancers, ACS Appl. Mater. Interfaces 11 (8) (2019) 7731–7742, https://doi.org/10.1021/acsami.8b19840.

[15] D. Brevet, M. Gary-Bobo, L. Raehm, S. Richeter, O. Hocine, K. Amro, B. Loock, P. Couleaud, C. Frochot, A. Morere, P. Maillard, M. Garcia, J.O. Durand, Mannose-targeted mesoporous silica nanoparticles for photodynamic therapy, Chem. Commun. (Camb. Engl.) 12 (2009) 1475–1477, https://doi.org/10.1039/b900427k.

[16] Y.C. Chang, A.C. Del Valle, H.P. Yeh, Y. He, Y.F. Huang, Development of photo-activated ROS-Responsive nanoplatform as a dual-functional drug carrier in combinational chemo-photodynamic therapy, Front. Chem. 6 (2018) 647, https://doi.org/10.3389/fchem.2018.00647.

[17] M.J. Abeledo-Lameiro, E. Ares-Mazas, H. Gomez-Couso, Evaluation of solar photocatalysis using TiO2 slurry in the inactivation of Cryptosporidium parvum oocysts in water, J. Photochem. Photobiol. B, Biol. 163 (2016) 92–99, https://doi.org/10.1016/j.jphotobiol.2016.08.016.

[18] C. Li, Y. Rao, B. Zhang, K. Huang, X. Cao, D. Peng, J. Wu, L. Xiao, Y. Huang, Extraordinary catalysis induced by titanium foil cathode plasma for degradation of water pollutant, Chemosphere 214 (2019) 341–348, https://doi.org/10.1016/j.chemosphere.2018.09.138.

[19] H. Adamu, M. Shand, R.S.F. Taylor, H.G. Manyar, J.A. Anderson, Use of carbon-based composites to enhance performance of TiO2 for the simultaneous removal of nitrates and organics from aqueous environments, Environ. Sci. Pollut. Res. Int. 25 (32) (2018) 32001–32014, https://doi.org/10.1007/s11356-018-3120-x.

[20] B. Xi, L.K. Verma, J. Li, C.S. Bhatia, A.J. Danner, H. Yang, H.C. Zeng, TiO2 thin films prepared via adsorptive self-assembly for self-cleaning applications, ACS Appl. Mater. Interfaces 4 (2) (2012) 1093–1102, https://doi.org/10.1021/am201721e.

[21] L. Yao, J. He, Z. Geng, T. Ren, Fabrication of mechanically robust, self-cleaning and optically high-performance hybrid thin films by SiO(2)&TiO(2) double-shelled hollow nanospheres, Nanoscale 7 (30) (2015) 13125–13134, https://doi.org/10.1039/c5nr02467f.

[22] H.X. Zhu, P.X. Zhou, X. Li, J.M. Liu, Electronic structures and optical properties of rutile TiO2 with different point defects from DFT + U calculations, Phys. Lett. A 378 (36) (2014) 2719–2724, https://doi.org/10.1016/j.physleta.2014.07.029.

[23] C. Chen, P. Li, G. Wang, Y. Yu, F. Duan, C. Chen, W. Song, Y. Qin, M. Knez, Nanoporous nitrogen-doped titanium dioxide with excellent photocatalytic activity under visible light irradiation produced by molecular layer deposition, Angew. Chem. Int. Ed. Engl. 52 (35) (2013) 9196–9200, https://doi.org/10.1002/anie.201302329.

[24] R. Asahi, T. Morikawa, T. Ohwaki, K. Aoki, Y. Taga, Visible-light photocatalysis in nitrogen-doped titanium oxides, Science 293 (5528) (2001) 269–271, https://doi.org/10.1126/science.1061051.

[25] I. Milosevic, S. Rtimi, A. Jayaprakash, B. van Driel, B. Greenwood, A. Aimable, M. Senna, P. Bowen, Synthesis and characterization of fluorinated anatase nanoparticles and subsequent N-doping for efficient visible light activated photocatalysis, Colloids Surf. B Biointerfaces 171 (2018) 445–450, https://doi.org/10.1016/j.colsurfb.2018.07.035.

[26] P. Junlabhut, C. Wattanawikkam, W. Mekprasart, W. Pecharapa, Effect of metal (Mn, Co, Zn, Ni) doping on structural, optical and photocatalytic properties of TiO (2) nanoparticles prepared by sonochemical method, J. Nanosci. Nanotechnol. 18 (10) (2018) 7302–7309, https://doi.org/10.1166/jnn.2018.15717.

[27] C. Liu, F. Wang, S. Zhu, Y. Xu, Q. Liang, Z. Chen, Controlled charge-dynamics in cobalt-doped TiO2 nanowire photoanodes for enhanced photoelectrochemical water splitting, J. Colloid Interface Sci. 530 (2018) 403–411, https://doi.org/10.1016/j.jcis.2018.07.003.

[28] D.T. Nguyen, S.S. Hong, Synthesis of metal ion-doped TiO2 nanoparticles using two-phase method and their photocatalytic activity under visible light irradiation, J. Nanosci. Nanotechnol. 16 (2) (2016) 1911–1915.

[29] B. Chen, B.W. Pogue, T. Hasan, Liposomal delivery of photosensitising agents, Expert Opin. Drug Deliv. 2 (3) (2005) 477–487, https://doi.org/10.1517/17425247.2.3.477.

[30] M.R. Hamblin, Fullerenes as photosensitizers in photodynamic therapy: pros and cons, Photochem. Photobiol. Sci. 17 (11) (2018) 1515–1533, https://doi.org/10.1039/c8pp00195b.

[31] X. Wang, J. Li, Y. Wang, L. Koenig, A. Gjyrezi, P. Giannakakou, E.H. Shin, M. Tighiouart, Z.G. Chen, S. Nie, D.M. Shin, A folate receptor-targeting nanoparticle minimizes drug resistance in a human cancer model, ACS Nano 5 (8) (2011) 6184–6194, https://doi.org/10.1021/nn200739q.

[32] S.N. Shah, Z. Shah, M. Hussain, M. Khan, Hazardous effects of titanium dioxide nanoparticles in ecosystem, Bioinorg. Chem. Appl. 2017 (2017) 4101735, , https://doi.org/10.1155/2017/4101735.

[33] S. Wang, L. Ji, B. Wu, Q. Gong, Y. Zhu, J. Liang, Influence of surface treatment on preparing nanosized TiO2 supported on carbon nanotubes, Appl. Surf. Sci. 255 (5, Part 2) (2008) 3263–3266, https://doi.org/10.1016/j.apsusc.2008.09.031.

[34] T.R. Gordon, M. Cargnello, T. Paik, F. Mangolini, R.T. Weber, P. Fornasiero, C.B. Murray, Nonaqueous synthesis of TiO2 nanocrystals using TiF4 to engineer morphology, oxygen vacancy concentration, and photocatalytic activity, J. Am. Chem. Soc. 134 (15) (2012) 6751–6761, https://doi.org/10.1021/ja300823a.

[35] O. Mitsunobu, The use of diethyl azodicarboxylate-triphenylphosphine system in the synthesis and transformation of natural products, in: W.J. Stec (Ed.), Phosphorus Chemistry Directed Towards Biology, Pergamon, 1980, pp. 213–218, , https://doi.org/10.1016/B978-0-08-023969-9.50025-1.

[36] M. Horie, S. Sugino, H. Kato, Y. Tabei, A. Nakamura, Y. Yoshida, Does photocatalytic activity of TiO2 nanoparticles correspond to photo-cytotoxicity? Cellular uptake of TiO2 nanoparticles is important in their photo-cytotoxicity, Toxicol. Mech. Methods 26 (4) (2016) 284–294, https://doi.org/10.1080/15376516.2016.1175530.

[37] L. Cano-Casanova, A. Amoros-Perez, M.A. Lillo-Rodenas, M.D.C. Roman-Martinez, Effect of the preparation method (Sol-Gel or hydrothermal) and conditions on the TiO(2) properties and activity for propene oxidation, Mater. Basel (Basel, Switzerland) 11 (11) (2018), https://doi.org/10.3390/ma11112227.

[38] B.K. Mutuma, G.N. Shao, W.D. Kim, H.T. Kim, Sol–gel synthesis of mesoporous anatase–brookite and anatase–brookite–rutile TiO2 nanoparticles and their photocatalytic properties, J. Colloid Interface Sci. 442 (2015) 1–7, https://doi.org/10.1016/j.jcis.2014.11.060.

[39] A. Garg, T. Singhania, A. Singh, S. Sharma, S. Rani, A. Neogy, S.R. Yadav, V.K. Sangal, N. Garg, Photocatalytic degradation of Bisphenol-A using N, Co

codoped TiO2 catalyst under solar light, Sci. Rep. 9 (1) (2019) 765, https://doi.org/10.1038/s41598-018-38358-w.
[40] R. Nunes, F. Araújo, J. Tavares, B. Sarmento, J. das Neves, Surface modification with polyethylene glycol enhances colorectal distribution and retention of nanoparticles, Eur. J. Pharm. Biopharm. 130 (2018) 200–206, https://doi.org/10.1016/j.ejpb.2018.06.029.
[41] J.S. Suk, Q. Xu, N. Kim, J. Hanes, L.M. Ensign, PEGylation as a strategy for improving nanoparticle-based drug and gene delivery, Adv. Drug Deliv. Rev. 99 (Pt A) (2016) 28–51, https://doi.org/10.1016/j.addr.2015.09.012.
[42] Y. Wang, H. Cui, J. Zhou, F. Li, J. Wang, M. Chen, Q. Liu, Cytotoxicity, DNA damage, and apoptosis induced by titanium dioxide nanoparticles in human non-small cell lung cancer A549 cells, Environ. Sci. Pollut. Res. - Int. 22 (7) (2015) 5519–5530, https://doi.org/10.1007/s11356-014-3717-7.
[43] X. Zhao, L. Sheng, L. Wang, J. Hong, X. Yu, X. Sang, Q. Sun, Y. Ze, F. Hong, Mechanisms of nanosized titanium dioxide-induced testicular oxidative stress and apoptosis in male mice, Part. Fibre Toxicol. 11 (2014), https://doi.org/10.1186/s12989-014-0047-3 47-47.
[44] S.N.A. Shah, Z. Shah, M. Hussain, M. Khan, Hazardous effects of titanium dioxide nanoparticles in ecosystem, Bioinorg. Chem. Appl. 2017 (2017) 12, https://doi.org/10.1155/2017/4101735.
[45] C.W. Dunnill, I.P. Parkin, Nitrogen-doped TiO2 thin films: photocatalytic applications for healthcare environments, Dalton Trans. 40 (8) (2011) 1635–1640, https://doi.org/10.1039/c0dt00494d.
[46] R.L. Siegel, K.D. Miller, A. Jemal, Cancer statistics, 2015, CA Cancer J. Clin. 65 (1) (2015) 5–29, https://doi.org/10.3322/caac.21254.
[47] R.L. Siegel, K.D. Miller, A. Jemal, Cancer statistics, 2019, CA Cancer J. Clin. 69 (1) (2019) 7–34, https://doi.org/10.3322/caac.21551.
[48] C. Thallinger, T. Fureder, M. Preusser, G. Heller, L. Mullauer, C. Holler, H. Prosch, N. Frank, R. Swierzewski, W. Berger, U. Jager, C. Zielinski, Review of cancer treatment with immune checkpoint inhibitors : Current concepts, expectations, limitations and pitfalls, Wien. Klin. Wochenschr. 130 (3-4) (2018) 85–91, https://doi.org/10.1007/s00508-017-1285-9.
[49] J.S. Suk, Q. Xu, N. Kim, J. Hanes, L.M. Ensign, PEGylation as a strategy for improving nanoparticle-based drug and gene delivery, Adv. Drug Deliv. Rev. 99 (Pt A) (2016) 28–51, https://doi.org/10.1016/j.addr.2015.09.012.